Study of Core Transport of Intrinsic Impurities in ELM-free NSTX Discharges with Lithium Wall Conditioning

F. Scotti[1], V.A. Soukhanovskii[2], R.E. Bell[1], M. Podesta[1], W. Guttenfelder[1], S. Gerhardt[1], R. Kaita[1], S. Kaye[1], B.P. LeBlanc[1] and the NSTX Team

[1]Princeton Plasma Physics Laboratory, Princeton, NJ, US
[2]Lawrence Livermore National Laboratory, Livermore, CA, US
Email contact of main author: fscotti@pppl.gov

Abstract:
Neoclassical transport of intrinsic impurities (carbon and lithium) is analyzed in H-mode discharges in NSTX. The application of lithium coatings on boronized graphite plasma facing components led to high performance H-mode discharges with edge localized modes (ELMs) suppression and resulted in core carbon accumulation. Lithium ions did not accumulate and had densities (n_{Li}) only up to 1% of carbon densities (n_C). Core transport codes NCLASS, NEO and MIST are used to assess the impact of wall conditioning via lithium evaporative coatings on impurity transport. The disappearance of ELMs together with changes in neoclassical transport due to modifications in main ion temperature (T_D) and density (n_D) profiles explains the core carbon accumulation. Residual anomalous transport is needed to explain the n_C profiles evolution. The enhancement in lithium particle diffusivities due to the presence of a strong impurity (carbon) can partially account for the low lithium core concentration.

1 Introduction

Impurity control is one of the major concerns for the applicability of high performance ELM(edge localized mode)-free regimes in current and future magnetic confinement devices. Due to constraints on the lifetime of divertor materials in ITER, the number and the size of ELMs will be limited, with potential consequences on impurity accumulation. The application of lithium evaporative coatings on the graphite plasma facing components (PFCs) in the National Spherical Torus Experiment (NSTX) led to longer H-mode discharges with increased stored energy, suppression of ELMs and a concomitant core impurity accumulation [1, 2]. The achievement of ELM-free H-mode regimes led to the possibility of studying impurity sources, transport, and particle balances without the complications associated with ELMs. Even if the graphite PFCs are coated with lithium evaporative coatings with typical thicknesses of hundreds of nanometers, significant carbon sputtering is still observed. Carbon is the main core impurity of NSTX H-mode plasmas with its contribution to core Z_{eff} increasing up to 3 through the discharge and its accumulation causing lack of density control. Lithium concentration in the core is negligible, contributing to Z_{eff} less then 0.005 [3]. Metal impurity accumulation is also observed, which leads to a core radiated power up to 50% of the injected power while contributing to Z_{eff} less than 0.4 [4]. In this paper we study the differences in impurity core and edge neoclassical transport regimes for the main intrinsic impurities (carbon and lithium) and their relevance to experimental transport levels.

2 Comparison of core transport of intrinsic impurities

Experimental measurements and analysis tools - In NSTX, core impurity densities (carbon and lithium) are measured by charge exchange (CX) recombination spectroscopy (CHERS, Li-CHERS) [3, 5]. Carbon densities (n_C) are obtained from the C VI n = 8-7 transition at 529.1 nm while lithium densities (n_{Li}) are inferred from the Li III n = 7-5 transition at 516.7 nm. Due to the contamination of the Li III CX line with a C VI line (n = 14-10), n_{Li} must be understood as an upper estimate of the core n_{Li}, typically within 50% [3].

In order to explain core impurity behavior in tokamaks, both neoclassical and anomalous transport typically need to be taken into account. However, in spherical tori (ST) impurity transport proved to be close to the neoclassical levels both in CDX-U ohmic L-mode [6] and in NSTX NBI-heated H-mode discharges [7, 8, 9]. In this work, the predicted and experimental

levels of impurity transport are evaluated using the transport codes NCLASS [10], NEO [11] and MIST [12]. The neoclassical transport codes NCLASS and NEO were used to derive neoclassical fluxes and transport coefficients in mixed-regime, multi-species plasmas (including C^{6+} and Li^{3+} species). NEO was run using the full linearized Fokker-Plank collisional operator [13] and with the inclusion of toroidal rotation effects on equilibrium densities and radial fluxes [14].

In particular, impurity toroidal velocities v_{tor} faster than thermal velocities v_{th} can cause poloidal redistribution of the impurity density and enhance neoclassical radial fluxes. In NSTX H-mode plasmas, carbon v_{tor} often exceeds v_{th} in the core region [5] and asymmetries between the high field side (HFS) and low field side (LFS) n_e profiles are usually observed and have been associated with centrifugal effects [15, 16]. This is important for this work since the experimental impurity peaking factors may differ if they are evaluated on the LFS or on the flux-surface-averaged profiles.

The NEO code is used to estimate poloidal asymmetries of the impurity and main ion densities. An example is shown in Figure 1 for a discharge analyzed later in this paper (129014, $v_{tor} \sim 1.75 v_{th}$ for r/a ≤ 0.5). NEO was run using only LFS profiles (r/a ≥ 0). The HFS n_D and n_C were calculated using NEO and n_e was derived from quasineutrality. NEO predicts a significant n_C redistribution (up to 40-50%) in the core with a negligible effect on the n_D profile. The reconstructed HFS profiles are in good agreement with the experimental profiles both for n_C (available only until r/a 0.2 on the HFS) and for n_e. In cases where the centrifugal effects can be important, the neoclassical peaking factors will then need to be compared to the experimental ones calculated on flux-surface-averaged profiles.

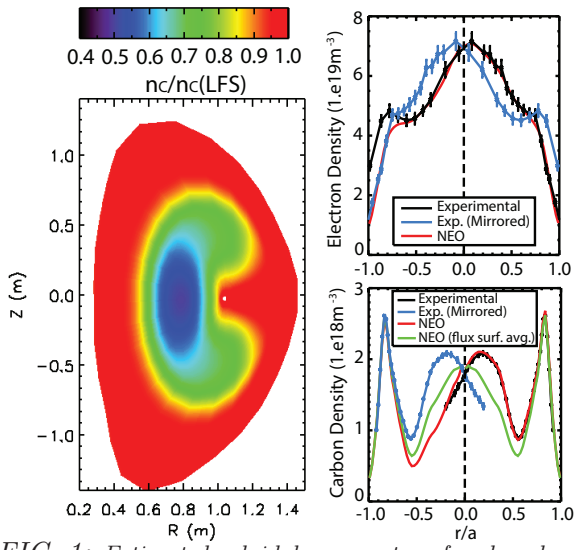

FIG. 1: Estimated poloidal asymmetry of carbon density (129014).

Comparison of neoclassical transport of lithium and carbon - In this section, the difference in neoclassical transport regimes for the two main impurities and their relevance to the experimental transport levels are compared. The analysis is based on H-mode, ELM-free, NBI-heated (4 MW) discharges with lithium evaporative coatings (170 mg). As shown in Figure 2, a low concentration (1%) peaked n_C profile in L-mode typically evolves into a hollow n_C profile at the H-mode transition with a steady slower accumulation in the core, concentrations up to 10% and profiles still evolving at the end of the discharge. A similar profile evolution is found for n_{Li} but with the extremely low values of 1% of core n_C as upper limit.

Collisionality regimes as well as collision frequencies and impurity strength factors are plotted in Figure 3. Deuterium ions are in the banana-plateau regime while both carbon and lithium ions are in plateau regime in the core and in Pfirsch-Schlüter (PS) regime for r/a larger than respectively 0.4 and 0.6. Lithium collision frequencies indicate the importance of including multi-ion effects [17, 18] for lithium transport. While carbon is a strong impurity (impurity strength $\alpha_C = n_C Z_C^2 / n_D \geq 5$ at $r/a \sim 0.8$) mostly collisional on deuterium ions ($\nu_{CD} \sim 10^4 s^{-1}$, $\nu_{CLi} \sim 5 \times 10^2 s^{-1}$), lithium is a trace impurity ($\alpha_{Li} \leq 0.02$ at $r/a \sim 0.8$), mostly collisional on background carbon ions ($\nu_{LiD} \sim 5 \times 10^3 s^{-1}$,$\nu_{LiC} \geq 10^4 s^{-1}$). For carbon, ambipolarity in the radial fluxes is satisfied to zeroth order in $\sqrt{m_e/m_D}$ with deuterium fluxes ($Z_C \cdot \Gamma_{r-C} =$ -Γ_{r-D}). Collisionality estimates and NCLASS indicate a negligible effect on carbon transport due to the presence of lithium ions. The low lithium concentrations allowed, using NCLASS, a sensitivity study on n_{Li} (between 0.01× and 100×$n_{Li\text{-}exp}$) with minor perturbation to the n_e

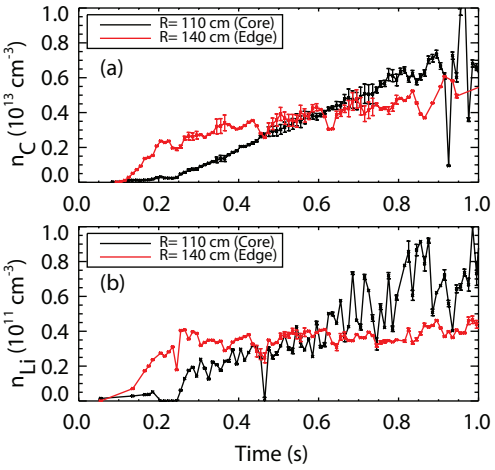

FIG. 2: (a) Carbon and (b) lithium density evolution (discharges 130725, 130727). Note difference in scale between (a) and (b).

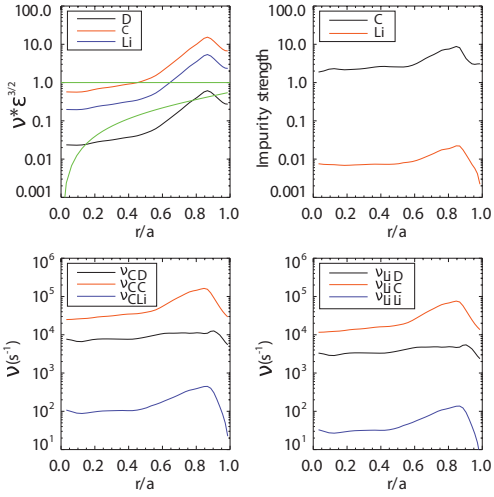

FIG. 3: Carbon and lithium transport regimes, collisionalities and impurity strength factors (130725, t=0.445s).

profiles (adjusted for quasi-neutrality). Effects on the neoclassical carbon transport can be seen only at $n_{Li} \sim 100 \times n_{Li\text{-}exp}$ as shown in Figure 4. Thus, lithium ions are not responsible for the increased carbon ion confinement and carbon transport is still mostly driven by main ions. Considering only the PS component of carbon transport due to friction on main ions [17, 18], we can write carbon radial fluxes as:

$$\Gamma^C_{PS} = \frac{q^2 n_D \rho_D^2 \nu_{DC}}{Z_C} \times \left[K \left(\frac{\partial ln n_D}{\partial r} - \frac{Z_D}{Z_C} \frac{\partial ln n_C}{\partial r} \right) + H \frac{\partial ln T_D}{\partial r} \right]. \quad (1)$$

In typical NSTX plasma conditions (main ion collisionality and impurity strength), $K \sim 1$ and $H \sim$ -0.5. The ∇T_D term provides a screening term, while a monotonically decreasing deuteron density (n_D) profile would lead to an inward term in the impurity flux. In NSTX H-mode discharges with lithium evaporative coatings, the edge ∇T_D is reduced and neoclassical carbon transport is then mostly driven by the ∇n_D term.

Lithium transport, on the other hand, is mostly driven by collisions on carbon ions. The high background carbon density leads to an increase in lithium particle diffusivities D_{Li}. From the Hirshmann-Sigmar formulation [17] for a trace impurity (lithium) in PS regime we can derive the contribution to D_{Li} due to a background impurity ($D_{Li\text{-}C}$) with respect to the one due to main ions ($D_{Li\text{-}D}$).

$$\frac{D^{PS}_{Li\text{-}C}}{D^{PS}_{Li\text{-}D}} = \frac{Y(m_{Li}/m_D) n_C Z_C^2 \sqrt{\frac{m_{Li}}{m_D}}}{n_D} \approx \frac{n_C Z_C^2}{n_D} \quad (2)$$

A carbon concentration of $\sim 3\%$ would cause a $\sim$100% enhancement of D_{Li}. This is consistent with NCLASS results: the high edge carbon concentrations ($\sim$ 10%) in ELM-free discharges lead to enhanced D_{Li} and reduced peaking factors (v_{Li}/D_{Li}). This is shown in Figure 5 where a sensitivity study in n_C is performed in subsequent NCLASS runs.

A comparison of neoclassical transport coefficients for carbon and lithium is shown in Figure 6. The transport coefficients are calculated from the impurity radial particle fluxes $\Gamma_{r\text{-}Z}$ via a scan in the impurity density gradient. Diffusivity (D) and convective velocity (v) are obtained from the slope and the intercept of the linear fit of $\Gamma_{r\text{-}Z}/n_Z$ versus -$\nabla n_Z/n_Z$ respectively and depend on the flux surface label choice (here the in-out r/a). One can see the difference in transport coefficients for carbon and lithium ions with lithium showing an order of magnitude higher edge D (Figure 6-a) with comparable or higher inward edge v (Figure 6-b). The outward di-

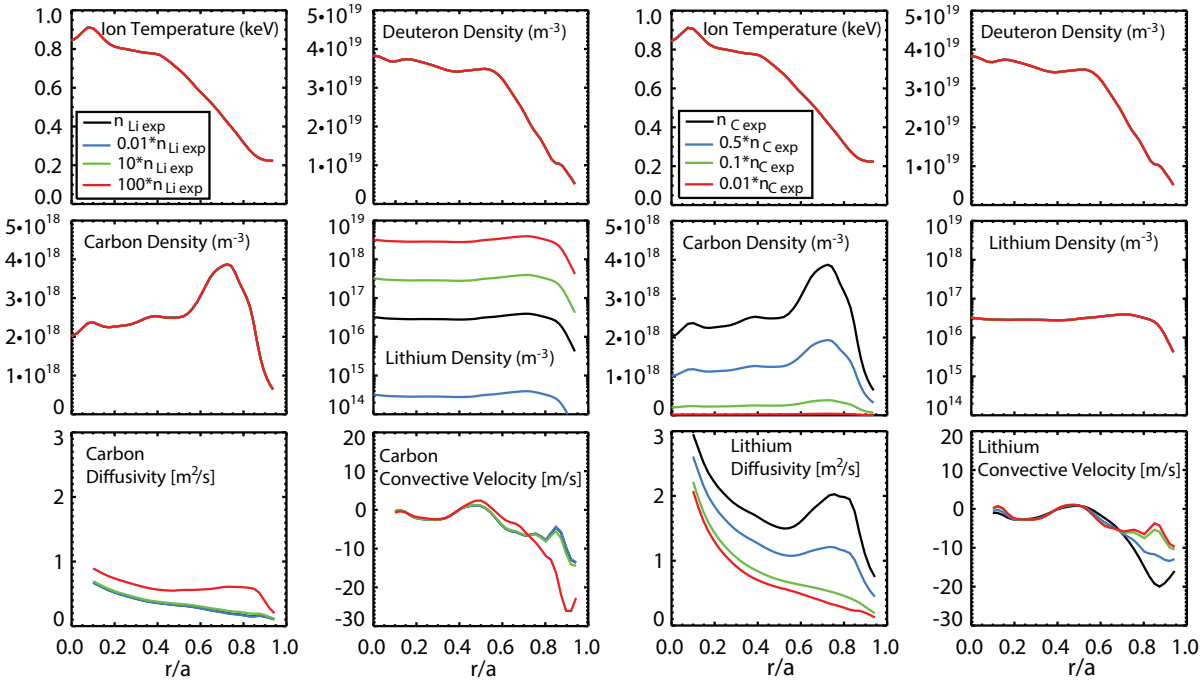

FIG. 4: Modeling of the effect of n_{Li} on neoclassical carbon transport coefficients.

FIG. 5: Modeling of the effect of n_C on neoclassical lithium transport coefficients.

rected lithium radial particle flux (Figure 6-c) for r/a ≥ 0.8 indicates that lithium edge fluxes are dominated by the diffusive component. NEO and NCLASS are in good agreement showing differences only inside of r/a=0.6 due to the effects of toroidal rotation that are neglected in NCLASS.

The relevance of neoclassical transport to the experimental transport levels can be investigated looking at the impurity peaking factors. Neoclassical predictions for the steady state peaking factors (v_{neo}/D_{neo}) can be compared to the experimental logarithmic impurity density gradients ($d(ln(n_z))/dr \sim v_{exp}/D_{exp}$) for both carbon and lithium in the source free region. Since the measured n_{Li} is as an upper estimate of the real n_{Li}, the profile shape and the gradient scale lengths might be only partially representative of the real n_{Li} profile. As shown in Figure 7, for both lithium and carbon in the early stages of the discharge the experimental v/D are in good agreement with the neoclassical estimates. Both NEO and NCLASS predict a large region (r/a ≤ 0.8) of outward convection which agrees with the experimentally observed hollow impurity profiles. Later in the discharge the neoclassical carbon peaking factor deviates from the experimental one: while the absolute values are comparable, neoclassical estimates predict the zero peaking position to be more inboard than observed experimentally. Possible reasons include residual anomalous transport, non-local effects in the core and in the steep gradient region not predicted by NEO and possible uncertainties in the n_D profiles which are indirectly measured from n_e assuming quasineutrality between e^-, D^+ and C^{6+}. Lithium behavior seems to be

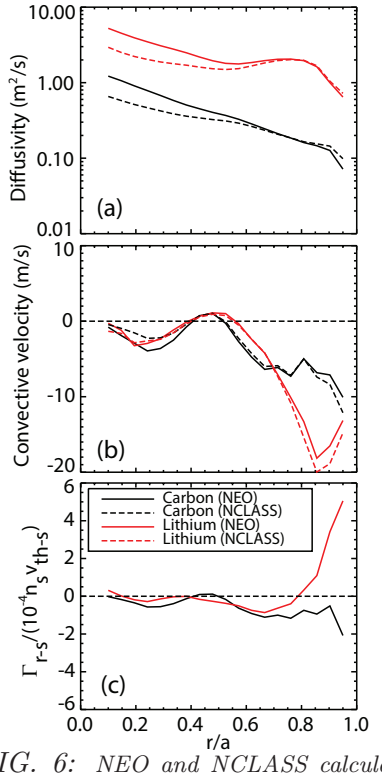

FIG. 6: NEO and NCLASS calculation of radial transport coefficients

closer to neoclassical predictions, possibly due to the higher neoclassical particle diffusivities.

The differences in core neoclassical transport for the two impurities can lead to differences in the core concentrations for carbon and lithium. The carbon and lithium transport differences were modeled using the MIST code [12] in a predictive mode. Using the experimental T_e and n_e, the time dependent neoclassical transport coefficients for carbon and lithium calculated by NCLASS were used to predict the time evolution of the charge state distribution of the two impurities given the same edge impurity source. The source was assumed to be a singly ionized source at the separatrix consistent with the temporal evolution of divertor impurity influxes. The same transport coefficients were assumed for all the charged states. MIST uses a simplified treatment of the edge source: the SOL is characterized using a constant perpendicular diffusivity (D_{SOL}) and convective velocity equal to the value at the separatrix and a parallel loss time ($\tau_{\|}$). Two scenarios were applied: the first using the same $\tau_{\|}$ for both impurities and the second using $\tau_{\|} = \lambda_{SOL}^2/D_{SOL}$ where λ_{SOL} is the characteristic SOL scale length. Modeling with the MIST code shows how the higher D_{Li} results in core n_{Li} that varies between $\sim 30\%$ and several % of n_C, with n_{Li}/n_C decreasing with the increase in n_C over time. The low n_{Li} observed with MIST modeling is only qualitatively consistent with the extremely low n_{Li} observed experimentally as well as with the decrease of the lithium-to-carbon inventory ratio as the discharge progresses. Experimentally measured n_{Li} are usually 1% of n_C or less since the early phase of the discharge indicating the need for a reduction of $\sim$ an order of magnitude of the edge lithium sources if compared to carbon.

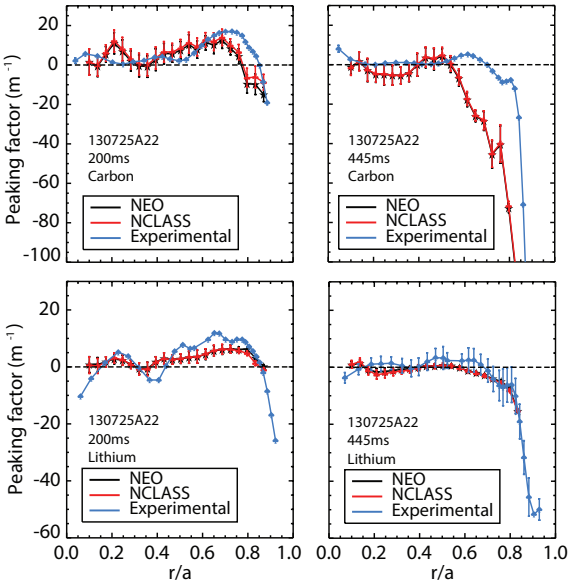

FIG. 7: Peaking factors for carbon (top) and lithium (bottom) for 130725 at t=200ms (left) and t=445 ms (right)

3 Changes in core carbon transport with the application of lithium evaporative coatings

In this section, the changes in carbon transport between discharges with boronized PFCs and lithiated PFCs are studied, including the role of changes in neoclassical transport and of the disappearance of ELMs. In Figure 8, waveforms from three discharges are shown, with same shaping, NBI heating and plasma current (900kA): a discharge with boronized PFCs without any lithium applied beforehand (in black), a discharge run after 8 grams of lithium had been cumulatively evaporated in previous discharges but without any fresh lithium (in blue) and a discharge with 190 mg of fresh lithium deposited before the discharge (in red). Looking at the lower divertor D_α, the progressive reduction in recycling and disappearance of ELMs is evident. The latter was associated with changes in the pedestal electron pressure profiles [2]. Medium size type-I ELMs in the discharge with boronized PFCs evolve into smaller ELMs in the intermediate discharge and disappear in the discharge with fresh lithium. Analysis of particle inventories show how discharges with lithium application result in an increase in core carbon inventories by as much as a factor of 3-4. Spectroscopic analysis of divertor carbon emission does not indicate an increase of carbon influxes with the application of lithium coatings, suggesting an improvement in core impurity confinement.

The changes in neoclassical core carbon transport due to lithium conditioning will now be examined. The contribution of lithium ions to carbon transport can be neglected. Changes

in neoclassical carbon transport are then related only to how lithium conditioning changes the main ion temperature T_D and density n_D profiles. Typical changes in ion profiles in discharges with lithium coatings with respect to discharges with boronized PFCs are an increase in n_C, an increase in the edge T_i, a reduction in n_D and its wider edge gradient. These changes can be seen in Figure 9, where the experimental profiles for the discharge without and with lithium are plotted together with the smoothed profiles used as input for the neoclassical analysis. The red band ($0.9 \leq r/a \leq 1.0$) indicates the area where extrapolation of the experimental profiles was done. The main drivers for carbon neoclassical transport are the edge ∇T_D and ∇n_D components. The reduction in the edge ∇T_D (screening) component and the wider ∇n_D component lead to a wider edge inward pinch that extends inward to r/a of 0.6 in discharges with lithium conditioning. For comparison, in boronized discharges the region with inward convective velocity would extend as far as r/a $\sim$ 0.8 as shown in Figure 10. Furthermore the change in the edge T_D and n_D leads to a change in the carbon edge particle diffusivity which is reduced by a factor of 2 at r/a $\sim$ 0.8. These changes in neoclassical transport are summarized in Figure 10 for discharges with and without lithium conditioning as calculated by NEO and NCLASS. Assuming the impurity transport is dominated by neoclassical transport, the

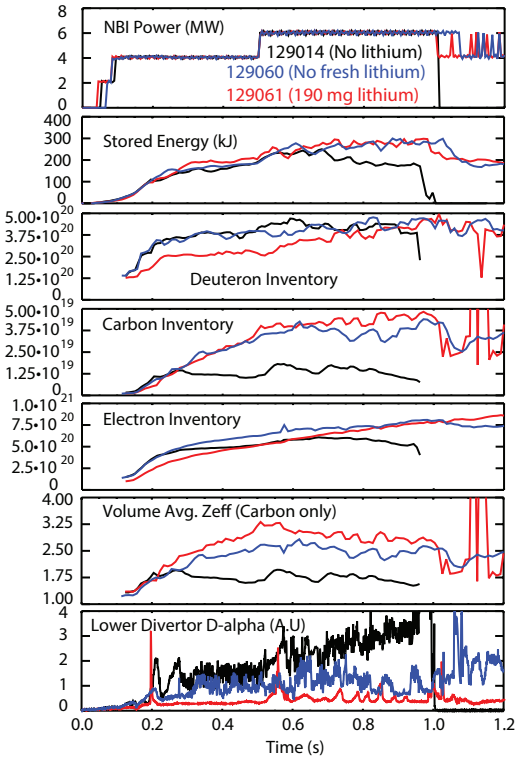

FIG. 8: Waveforms of discharge parameters and inventories with application of lithium coatings

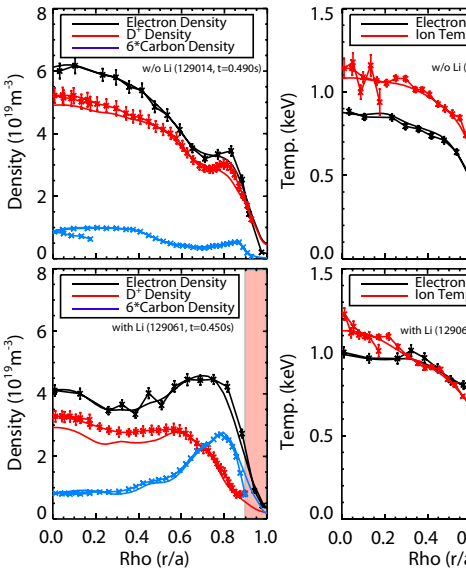

FIG. 9: Profiles for discharges without (TOP) and with (BOTTOM) lithium conditioning .

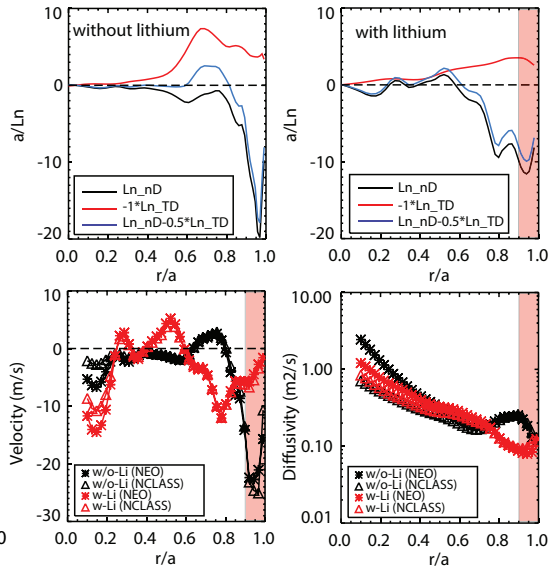

FIG. 10: Gradient scale lengths and carbon neoclassical transport coefficients with and w/o lithium.

change in the neoclassical transport coefficients with the application of lithium coatings leads to a change in the equilibrium n_C. The wider edge inward pinch and the core pinch would lead to

a higher penetration of carbon into the core region, if compared to discharges with boronization where carbon ions would remain concentrated in the region with r/a larger than 0.8 as seen in Figure 11 and 12. The experimental n_C and the n_C evolution as predicted by MIST, assuming neoclassical transport coefficients, are plotted versus radius and time for a discharge with boronized PFCs and a discharge with evaporative lithium coatings. The carbon edge source was

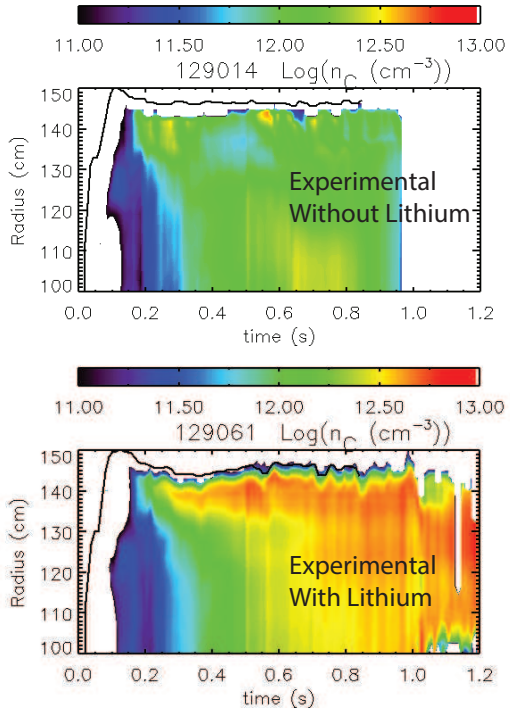

FIG. 11: Experimental carbon profiles for discharges without and with lithium conditioning.

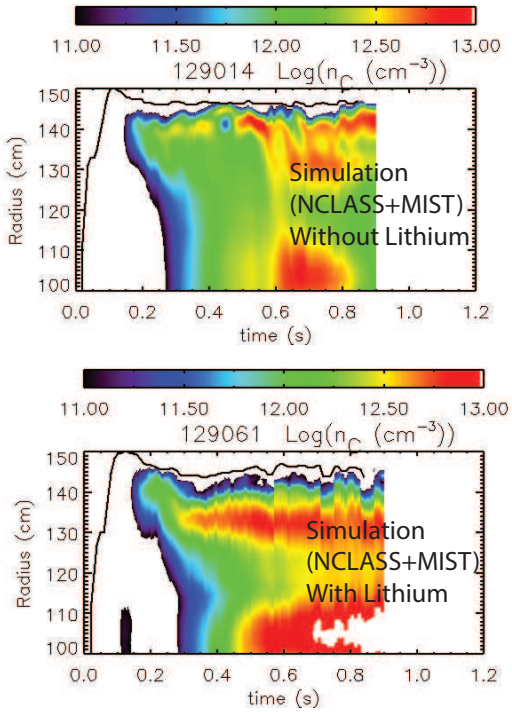

FIG. 12: Simulated carbon profiles for discharges without and with lithium conditioning.

assumed to be the same in the discharge with lithium coatings and in the one with boronized PFCs. The neoclassical prediction for the discharge with boronized PFCs is in reasonable agreement with the experimental profiles early in time and later develops strong peaking in the edge region, which is not observed experimentally. The calculated carbon inventory ramps during the discharge suggesting that the ELMs have an important role in keeping the edge carbon density and total carbon inventory flat versus time as observed experimentally. The neoclassical prediction for the discharge with lithium coatings again shows agreement in the early evolution of the discharge. For later times, neoclassical predictions indicate the location of the edge peaking to be more inboard than observed experimentally and greater core peaking than measured. These observations are also confirmed comparing the experimental peaking factors to the neoclassical predictions. While the profile evolution in discharges with lithium coatings is qualitatively consistent with neoclassical transport, some anomalous transport is still needed in order to explain experimental profiles. However, the change in the baseline neoclassical transport with lithium conditioning, would lead to a deeper penetration of the impurities in the core where they would be less sensitive to the flushing effect of ELMs. This is qualitatively consistent with the observation that ELMs triggered with 3D fields in discharges with lithium coatings were able to affect only the carbon density in the outer most volume of the plasma [19], leaving the central accumulation unaffected. Due to the large uncertainties in the n_D profiles for r/a larger than 0.9 in discharges with lithium conditioning, no conclusive answer can be given on the potential effect on the core inventories as a result of the change in edge neoclassical transport coefficients

only. ELMs in discharges without lithium conditioning appear to be responsible for keeping the total impurity inventory flat in time.

4 Summary

Intrinsic impurity (carbon and lithium) neoclassical transport is analyzed for H-mode discharges in NSTX. ELM-free H-mode discharges are generally characterized by carbon accumulation. Lithium ions do not accumulate and have densities (n_{Li}) only up to 1% of carbon densities (n_C). Core transport codes NCLASS, NEO and MIST were used to assess the impact of lithium conditioning on impurity transport. The disappearance of ELMs together with changes in neoclassical transport due to modifications in main ion temperature (T_D) and density (n_D) profiles can explain the core carbon accumulation. However, residual anomalous transport is needed in order to reproduce the evolution of the n_C profiles. The enhancement in lithium particle diffusivities due to the presence of carbon can partially account for the low lithium core contamination. A reduction of the edge source of an order of magnitude if compared to the carbon edge source would still be needed in order to reproduce the extremely low n_{Li} observed in experiments.

5 Acknowledgements

Work supported by U.S. DOE Contract DE-AC02-09CH11466 and DE-AC52-07NA27344. The authors would like to acknowledge Dr. Robert Andre for assistance with NCLASS, Dr. Steve Sabbagh for EFIT calculations, Dr. Rajesh Maingi, Dr. Eric Meier and Dr. Alessandro Bortolon for useful discussions, Dr. Emily Belli ans Dr. Jeff Candy for the availability of NEO code and useful discussions.

References

[1] M.G. Bell et al., Plasma Phys. Control. Fusion 51(12), 2009.
[2] R. Maingi, et al., Phys. Rev. Lett. 103 (7), 075001, 2009.
[3] M. Podesta, et al., Nucl. Fusion, 52, 033008, 2012.
[4] S.F. Paul, et al., J. Nucl. Mater. 390-91, 211-215, 2009.
[5] R.E. Bell, et al., Rev. Sci. Instrum., 81, 10D724, 2010.
[6] V. A. Soukhanovskii, et al., Plasma Phys. Contr. Fusion 44, 2339, 2002.
[7] L. Delgado-Aparicio, et al., Nucl. Fusion, 49(8):085028, 2009.
[8] L. Delgado-Aparicio, et al., Nucl. Fusion 51 (8) 083047, 2011.
[9] D. Clayton, et al. Submitted to Plasma Phys. Control. Fusion (2012).
[10] W.A. Houlberg et al., Phys. Plasmas 4 (9), 1997.
[11] E.A. Belli et al., Plasma Phys. Control. Fusion, 50, 095010, 2008.
[12] R. Hulse, Nucl. Technol. Fusion 3 (259), 1983.
[13] E.A. Belli et al., Plasma Phys. Control. Fusion, 51, 075018, 2009.
[14] E.A. Belli et al., Plasma Phys. Control. Fusion, 54, 015015, 2012.
[15] J.E. Menard, et al. Nucl. Fusion 45 539, 2005.
[16] S.P. Gerhardt, et al. Nucl. Fusion 51, 033004, 2011.
[17] S.P. Hirshmann et al., Nucl. Fusion, 21, 1079, 1981.
[18] K. Wenzel et al., Nucl. Fusion, 30, 1117, 1990.
[19] J.M. Canik, et al. Phys. Rev. Lett, 104 (4), 045001, 2010.